Probing crystallization of a fluoro-apatite - mullite system using neutron diffraction

J M Smith[1,2], R A Martin[3*], D T Bowron[4], A C Hannon[4], R J Newport[1].

[1] School of Physical Science, University of Kent, Canterbury, CT2 7NH, UK

[2] Central Laser Facility, STFC Rutherford Appleton Laboratory, Didcot, OX11 0QX, UK

[3] School of Engineering & Applied Science and Aston Research Centre for Healthy Ageing, Aston University, Birmingham, B4 7ET, UK

[4] ISIS Facility, Rutherford Appleton Laboratory, Didcot, Oxon OX11 0QX, UK

*Corresponding author.

E-mail address: R.A.Martin@Aston.ac.uk (R.A. Martin).

Abstract

Real-time small angle neutron scattering and wide angle neutron scattering studies were undertaken concurrently on a glass ionomer of nominal composition 4.5(SiO_2)-3(Al_2O_3)-1.5(P_2O_5)-3(CaO)-2(CaF_2). Neutron studies were conducted as a function of temperature to investigate the crystallisation process. No amorphous phase separation was observed at room temperature and the onset of crystallisation was found to occur at 650°C, which is 90°C lower than previously reported. The first crystalline phase observed corresponded to fluorapatite; it was only upon further heating was the mullite phase became present. The crystallite size at 650°C was found to be ~ 115 Å and the result was consistent across all measurements.

Introduction

Fluoro-apatite – mullite glasses are of considerable interest for dental applications [1]. Fluoride ions are essential for the formation of normal tooth and bone tissue [2]. Fluoride ions also prevent dental caries by enhancing mineralization, reducing demineralization and inhibiting bacterial enzymes [3]. Accordingly, fluorine has been incorporated into bioactive glass for dental cement applications [4]. For fluorine-containing cements fluorapatite is formed, rather than hydroxyapatite, under physiological conditions. Fluorapatite is known to be more chemically stable, particularly under acid attack which is of further benefit in dental applications [3]. Additional benefits of the incorporation of fluorine include the lowering of the glass transition temperature and extending the working time of the cement [5]. Consequently, these materials have been studied using a range of techniques including: scanning electron microscopy (SEM) [6], Dynamic Mechanical Thermal Analysis (DMTA) [7], computer modelling [8], NMR [9], Fourier transform infrared spectroscopy (FTIR), solid state MAS-NMR spectroscopy [9] and neutron diffraction [10]. Glass transition results showed two transition temperatures and demonstrated that the parent glass phase separates into two amorphous glass phases. The SEM results indicate that these phases are not interconnected and instead sparse calcium and fluoride rich droplets, on the scale of 20-100 nm, are dispersed in the matrix of enriched in aluminium and silicon and depleted in calcium and fluoride glass. There are well-defined interfaces which indicate no interconnectivity, and a random distribution which may possibly indicate phase separation [6].

The first step of crystallisation can be thought of as a nucleation phase [11]. The nucleation process tends to occur at temperatures only slightly higher than the glass transition temperature. However, nucleation has been observed to occur at lower temperatures if the length of time maintained at this temperature is extended; and as such a time dependence has been inferred for the process of nucleation [7]. In some homogeneous glasses the nucleation process begins with the separation into several phases. These phases have different compositions, and the separation of these phases may aid crystallisation. This glass has previously been reported to undergo bulk nucleation after amorphous phase separation [12].

The present study investigates the structure and the crystallization process of 4.5(SiO_2)-3(Al_2O_3)-1.5(P_2O_5)-3(CaO)-2(CaF_2), also known as LG26, as a function of temperature using simultaneous small and wide angle neutron diffraction. The conventional wide angle scattering was used to detect the onset of crystallisation by the emergence of Bragg peaks. Small angle scattering was used to observe the changing macrostructure, and in particular the effect of the evolving crystallisation on heating.

Method

Sample Preparation: amorphous 4.5(SiO_2)-3(Al_2O_3)-1.5(P_2O_5)-3(CaO)-2(CaF_2) was synthesized via the melt quench method. In brief, the precursors SiO_2 (Sigma Aldrich, 99.8%), Al_2O_3 (Sigma Aldrich, 99.99%), P_2O_5 (Sigma Aldrich, 99.99%), $CaCO_3$ (Alfa Aesar, 99.95%), $SrCO_3$ (Sigma Aldrich, 99.9%) and CaF_2 (Fisher Scientific, 99%), were weighed in the appropriate molar ratios and thoroughly mixed. The precursors were then placed in a Pt/Rh crucible and thence into a preheated furnace at 1450°C for one hour. The melt was cast into a preheated graphite mould at 450°C and then annealed overnight at this temperature before being slowly cooled to room temperature.

Sample Characterisation: X-ray diffraction was undertaken (using a Bruker D8 instrument) to ensure the samples were amorphous and that no crystallization had occurred during their fabrication. X-ray fluorescence was undertaken (PANalytical Epsilon 3) to determine the relative concentration of elements present in the sample; it must be noted that oxygen and fluorine cannot be detected using conventional benchtop X-ray florescence due to their low atomic number. We therefore assigned O and F to charge balance the measured values of P, Si, Ca and Al atoms that are detectable. In the case of Ca we assigned this to a mixture of CaO and CaF_2 whilst maintaining the initial starting ratio of fluoride to oxide. It is assumed, and has been confirmed in studies of glasses of similar composition, that the calcium carbonate decompose upon heating to produce calcium and that the calcium fluoride remains intact [12]. Weight loss measurements confirm the loss of carbonates from the melt derived sample. The sample densities were measured using helium pycnometry (Quantachrome Multi-Pycnometer). The glass transition temperature was measured using a NETZSCH STA 409 PG (TG/DSC) simultaneous thermal analysis, thermogravimetry, differential scanning calorimetry. Samples of ~ 30mg were heated in sealed aluminium pans at a rate of 5°C per minute up to 1000°C under standard atmosphere. Bioactive glasses are typically used in particulate form as filling agents. Our diffraction studies were undertaken on similarly powdered samples. Samples were ground using an agate pestle and mortar immediately prior to the diffraction studies to minimise any potential surface hydration effects.

Neutron diffraction: datasets were collected using the *Near and InterMediate Range Order Diffractometer* (NIMROD) [13] and the GEneral Materials diffractometer (GEM) [14] at the ISIS pulsed neutron source, Rutherford Appleton Laboratory. Diffraction datasets were collected at a series of temperatures using the instrument NIMROD, whilst room temperature measurements were conducted, for a series of pre-heat treated samples, using GEM.

NIMROD: The powdered samples were placed into thin walled flat-plate vanadium containers and heated *in situ* using the RAL-4 63mm bore furnace with vanadium windows mounted directly on the diffractometer. Diffraction patterns were collected at room temperature and at a series of predetermined elevated temperatures. The furnace was heated at a rate of 10°C/min until the sample was 10°C from the required temperature. To ensure the required temperature was not exceeded the heating rate was then reduced to 1°C/min for the final 10°C. In addition to the interference patterns collected for the samples, interference patterns were also collected for the empty instrument, empty sample container, a vanadium plate, and empty furnace to enable background corrections and normalization of the sample data to be achieved. Data reduction and normalisation were undertaken using the program *Gudrun* [15]. The Bragg peak free room temperature spectrum was Fourier transformed to give a real space function, D(r), and fitted using *NXFit* [16]. The corrected small angle scattering datasets were investigated using Guinier and Porod analysis [19].

GEM: Neutron datasets were collected for heat-treated samples using the GEM diffractometer. The samples were placed in cylindrical vanadium containers with inside diameter of 5.0 mm and a wall thickness of 0.025 mm. interference patterns for the empty instrument, vanadium rod and empty container were collected to allow for background and normalisation corrections. The datasets were corrected and normalised using *Gudrun* [15]. Bragg peaks were indexed using the Chemical Database Service database [17] to identify the crystal phases present in this system.

Results and Discussion

The resultant glass was optically transparent and visibly homogenous with no visible sign of crystallisation. X-ray diffraction data confirmed that the glasses were indeed amorphous. It is worth noting that previous studies traditionally quench these types of glasses into water to avoid crystallisation [12]. However, due to the need to undertake neutron diffraction experiments on these samples, all efforts were undertaken to ensure minimal surface hydration given that hydrogen is a strong inelastic scattering atom. This result demonstrates that these types of glasses can be prepared via conventional air quenching. The resulting composition, as determined by fluorescence spectroscopy, is given in Table 1. As seen there is reasonable agreement between the expected nominal composition and the experimentally measured composition (given an estimated 2% experimental error). The density of the fluoro-apatite – mullite glass was found to be 2.70 $g.cm^{-3}$ which is in agreement with the previously reported value of 2.73 $g.cm^{-3}$ [18].

Table 1. Composition of the fabricated glass (molar percent), estimated errors are ~ ±2%. Oxygen and fluorine compositions are inferred on the basis of charge-balancing the sample, and the ratio of CaO:CaF_2 maintained at the batch value.

	Nominal composition	Measured composition
SiO_2	32.1	30.6
P_2O_5	10.7	10.9
Al_2O_3	21.4	19.1
CaO	21.4	23.6
CaF_2	14.3	15.8

The real space data obtained from NIMROD, formed after applying background corrections and Fourier transforming the interference function $i(Q)$, is shown in Figure 1. As shown, there are no Bragg peaks present and the sample is fully amorphous prior to heat treatment. A preliminary fit confirms that the normalisation and background corrections have been correctly undertaken. For example the P-O and Si-O correlations are observed ~1.5 and 1.6 Å respectively and both have coordination numbers of ~ 4. The Al-O coordination occupies a mixture of tetrahedral and octahedral environments which is consistent with published ^{27}Al MAS-NMR results given by Hill *et al* who demonstrated that aluminium is present in 4-, 5- and 6-fold coordinations. It was observed by Hill *et al* that the aluminium environment is linked to the fluorine content, and an increase in the fluorine concentration results in an increase in 6-fold coordinated aluminium [9]. An exact ratio of Al environments cannot be determined due to the overlapping correlation functions.

The differential scattering cross section data as a function of temperature is shown in Figure 2. Small angle and wide angle regions are highlighted in Fig 2a and 2b respectively. It is apparent that samples remain amorphous up until ~600°C. There are no obvious signs of amorphous phase separation at room temperature, which is in contrast to results reported by Hill *et al* [10]. However, it is worth noting that the method of preparation was significantly different: Hill *et al* re-melted their samples to manufacture bulk rods, which may have been more susceptible to crystallisation, and given the uncertainties involved in its determination there may be small differences in composition. At 650°C the first signs of partial crystallisation are observed. A shoulder appears in the small angle data and small Bragg peaks can be observed on the top of the interference function peaks. As the temperature increases further the number and size of the Bragg peaks increases in the wide angle data. The position of the shoulder in the small angle data increases in intensity and shifts to smaller Q values (representing longer real-space distances) indicating the size of the crystallites are increasing. At 800 and 900°C the shoulder is no longer observable in the small angle scattering spectra; this is attributed to the increase in crystal size which means the feature is now outside of the reciprocal space measurement window available. It is possible to estimate the associated real space length scales, r, according to $r \sim 2\pi/Q$: at 650 and 700°C Q ~0.04 Å^{-1} therefore r ~ 150 Å; at 750°C Q ~0.03 Å^{-1} therefore r ~ 210 Å. The results are consistent with higher temperatures causing increased crystallisation and larger crystallites.

It is noted that the first signs of crystallisation occur at 650°C which is only 10°C above the glass transition temperature and 90°C lower than previously reported first crystallisation temperature determined by DSC measurements [12]. However, the present samples were powdered and therefore likely to be more susceptible to surface crystallisation. To further validate this result the sample heated to 650°C was held at that temperature for an extended time period before cooling to room temperature and subjected to re-measurement. The results are presented in Figure 3: after heating a large shoulder has developed ~0.05 Å^{-1} in the small angle data and small Bragg peaks appear at ~ 0.78, 1.6, 1.8 and 2.8 Å^{-1} which are irreversible, confirming that the samples have indeed undergone partial crystallisation.

The evolution of crystallisation was investigated as a function of a single fixed temperature (800°C). This temperature was selected since it is lies between the first (740°C) and second (930°C) reported crystallisation temperatures of LG26 [12]. This should allow only the first crystallisation phase to be examined. The sample was heated from room temperature to 800°C at a rate of 10°C per minute, apart from the last 10°C which was traversed at 1°C per minute to allow for thermal stabilisation and to avoid rising above the desired temperature. A diffraction pattern was then collected for each of

three successive 15 minute intervals. These three diffraction patterns were collected and analysed under identical conditions, the only variable being the cumulative amount of time each pattern had been held at 800°C. At 800°C Bragg peaks are visible at 0.76, 1.6, 1.81, 2.25 and 2.76 $Å^{-1}$ which are indicative of fluorapatite.

Diffraction patterns obtained for the samples after heating to 950°C, using the GEM instrument are shown in Figure 4. The peaks indicate the presence of mullite ($2SiO_2 \cdot 3Al_2O_3$) and fluorapatite ($Ca_5(PO_4)_3F$) crystalline phases [17].

The width of the Bragg peaks is dependent on several factors but most importantly, particularly at low *Q*-values, are the resolution of the instrument and the size of the crystallite causing the Bragg peaks. Determining the width of these peaks therefore provides an estimation of the size of the crystallite if one takes into account the known and constant resolution of the instrument, and a change in peak widths must be due to a change in crystallite size. Figure 5 shows the Gaussian peak width as a function of peak position for several of the Bragg peaks in the 950°C spectrum. The peak width increases with peak position: ΔQ increases in an approximately linear fashion as function of Q^2.

The width of the 0.7 $Å^{-1}$ Bragg peak was used to estimate the crystallite size as a function of temperature. Figure 6 illustrates the calculated crystallite size. At 650°C the crystallite size is calculated to be 125 Å and 950°C the crystallite size has grown to 203 Å. The resolution of the detector bank, and corresponding particle size resolution, is estimated to be 4% [13].

Small angle neutron scattering data was also used to determine the crystallite size through the application of Guinier analysis. Figure 7 illustrates the Guinier plot for samples heated to 650, 700 and 750°C. There is a small shoulder present on the 700°C plot at 0.0003 $Å^{-2}$, as indicated by the arrow. The position of the shoulder was estimated by first subtracting the background slope and then applying a least squares fitting routine. The location of the shoulder allows an approximation of the correlation length to be estimated as $R_g \sim 2\pi/Q$, this corresponds to $R_g \sim 115$ Å which is in good agreement with the value obtained from the Bragg peak width analysis. The small angle neutron scattering did not reveal an extended linear region for some of the higher temperatures and there was no detectable shoulder so no further information has been extracted for these samples.

Figure 8 illustrates the small angle neutron scattering data when plotted using the Porod method. The Porod plots have a similar initial gradient of approximately -4, this is indicative of large structures causing the scattering. This is expected, as the sample is a powder: the small angle scattering detected is highly likely to be dominated by the surface scattering of the grains of powder. However, at temperatures of 650 and 700°C a feature, super-imposed on the slope, is present. The gradient of the slope for these temperatures also changes from ~-4 to ~-2, the latter being indicative of the presence of mass fractals. The peak appearing at -2.9 in the spectrum for the 650°C sample corresponds to a structural motif with a size of $R_g \sim 114$ Å, which is in excellent agreement with the result obtained using the Guinier plot and the Bragg peak width analysis. It is apparent when comparing the spectra taken at 650 and 700°C that the peak in the Porod plot appears in the same position, the only difference between these temperatures is the amplitude of the peak, which is greater at the higher temperature.

Conclusion

The structure of powdered 4.5(SiO_2)-3(Al_2O_3)-1.5(P_2O_5)-3(CaO)-2(CaF_2) was investigated over an extended length scale using the *Near and InterMediate Range Order Diffractometer* (NIMROD). Small angle neutron scattering data obtained using NIMROD was successfully analysed using the Guinier and Porod methods. Complementary data on crystallite size was also obtained using the GEneral Materials diffractometer (GEM) via estimation of the Bragg peak widths. The results were found to be in excellent agreement. The first signs of crystallisation were observed at 650°C, which is 90°C below the previously reported value of 740°C obtained using differential scanning calorimetry. The crystallite size at 650°C is estimated to be ~ 115 Å and this is seen to increase to ~ 200 Å at 950°C.

Acknowledgements

We would like to acknowledge the STFC's ISIS the Pulsed Neutron Source for the allocation of beam-time and Professor Alan Soper for assistance with the NIMROD beam-time; we gratefully acknowledge the 'Next Generation Facility Users' studentship (JMS) and other support afforded by EPSRC award EP/F021011.

References

[1] Hill R, Wood D. APATITE MULLITE GLASS-CERAMICS. Journal of Materials Science-Materials in Medicine 1995;6:311-8.
[2] Jha LJ, Best SM, Knowles JC, Rehman I, Santos JD, Bonfield W. Preparation and characterization of fluoride-substituted apatites. Journal of materials science Materials in medicine 1997;8:185-91.
[3] Brauer DS, Al-Noaman A, Hill RG, Doweidar H. Density–structure correlations in fluoride-containing bioactive glasses. Materials Chemistry and Physics 2011;130:121-5.
[4] Mollazadeh S, Javadpour J, Yekta BE, Jafarzadeh TS, Youssefi A. Synthesis and characterisation of dental composite materials reinforced with fluoroapatite-mullite glass-ceramic particles. Advances in Applied Ceramics 2013;112:294-300.
[5] Stanton K, Hill R. The role of fluorine in the devitrification of SiO2·Al2O3·P2O5·CaO·CaF2 glasses. Journal of Materials Science 2000;35:1911-6.
[6] Rafferty A, Hill R, Kelleher B, O'Dwyer T. An investigation of amorphous phase separation, leachability and surface area of an ionomer glass system and a sodium-boro-silicate glass system. Journal of Materials Science 2003;38:3891-902.
[7] Rafferty A, Hill R, Wood D. Amorphous phase separation of ionomer glasses. Journal of Materials Science 2000;35:3863-9.
[8] Christie JK, Pedone A, Menziani MC, Tilocca A. Fluorine Environment in Bioactive Glasses: ab Initio Molecular Dynamics Simulations. Journal of Physical Chemistry B 2011;115:2038-45.
[9] Hill RG, Stamboulis A, Law RV. Characterisation of fluorine containing glasses by F-19, Al-27, Si-29 and P-31 MAS-NMR spectroscopy. Journal of Dentistry 2006;34:525-32.
[10] Hill R, Calver A, Stamboulis A, Bubb N. Real-Time Nucleation and Crystallization Studies of a Fluorapatite Glass–Ceramics Using Small-Angle Neutron Scattering and Neutron Diffraction. Journal of the American Ceramic Society 2007;90:763-8.
[11] Elliot S. The Physics and Chemistry of Solids 1998.
[12] Hill RG, Stamboulis A, Law RV, Clifford A, Towler MR, Crowley C. The influence of strontium substitution in fluorapatite glasses and glass-ceramics. Journal of Non-Crystalline Solids 2004;336:223-9.

[13] Bowron DT, Soper AK, Jones K, Ansell S, Birch S, Norris J, et al. NIMROD: The Near and InterMediate Range Order Diffractometer of the ISIS second target station. Review of Scientific Instruments 2010;81:033905.
[14] Hannon AC. Results on disordered materials from the GEneral Materials diffractometer, GEM, at ISIS. Nuclear Instruments & Methods in Physics Research Section a-Accelerators Spectrometers Detectors and Associated Equipment 2005;551:88-107.
[15] McLain SE, Bowron DT, Hannon AC, Soper AK. http://wwwisis2isisrlacuk/Disordered/Manuals/gudrun/Gudrun_manual_2006pdf.
[16] Pickup D, Moss R, Newport R. NXFit: a program for simultaneously fitting X-ray and neutron diffraction pair-distribution functions to provide optimized structural parameters. Journal of Applied Crystallography 2014;47:1790-6.
[17] http://icsd.cds.rsc.org/search/basic.xhtml. 2015.
[18] Kartelia EM. Thermal characterization of magnesium containing ionomer glasses 2011.

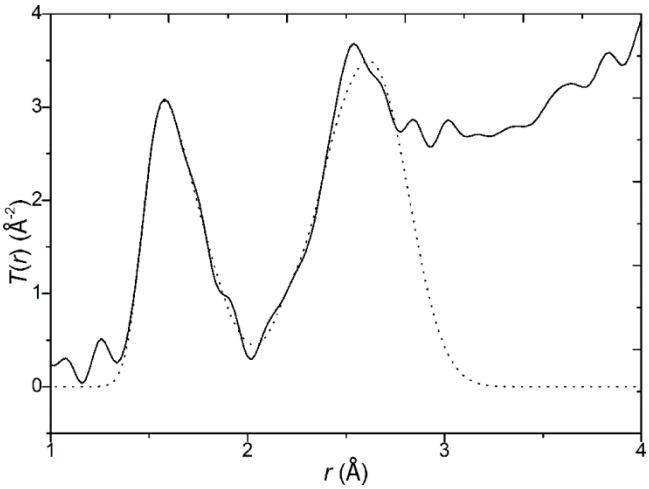

Figure1. The real space diffraction data obtained for fluoro-apatite – mullite glass at room temperature. The solid curve shows the experimental data and the dashed curve the fit.

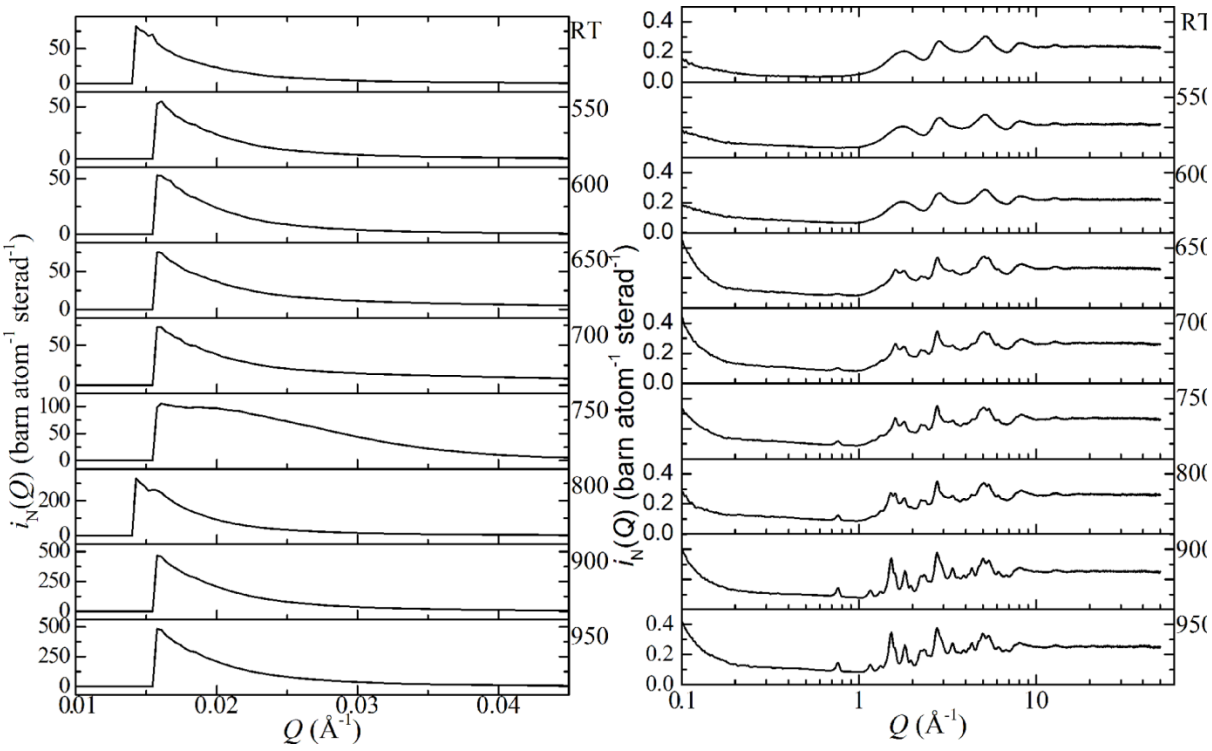

(a) (b)

Figure 2. The interference function as a function of temperature for (a) the small angle and (b) the wide angle regions.

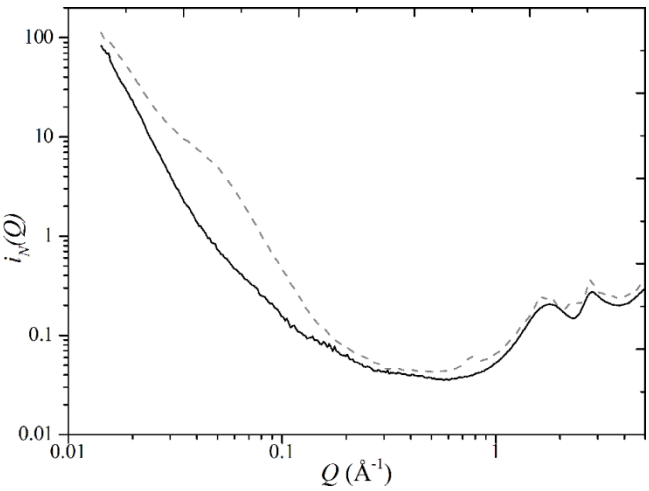

Figure 3: The differential scattering cross section data; the solid line represents the data collected at room temperature. The broken curve shows data for the same sample also collect at room temperature but after being pre-heated to 650°C and then cooled back to room temperature.

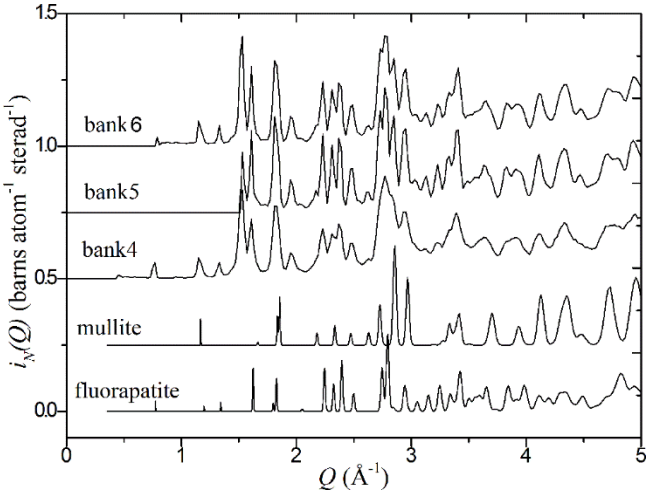

Figure 4: Diffraction patterns for fluoro-apatite – mullite glass after heating to 950°C obtained using GEM instrument over the Q-range 0.5 to 6 Å^{-1}. Detector banks 4, 5 and 6 are displayed individually offset by 0.5, 0.75 and 1.0 respectively. Diffraction patterns for mullite ($2SiO_2 \cdot 3Al_2O_3$) and fluorapatite ($Ca_5(PO_4)_3F$) are given for reference, mullite is offset by 0.25 for clarity.

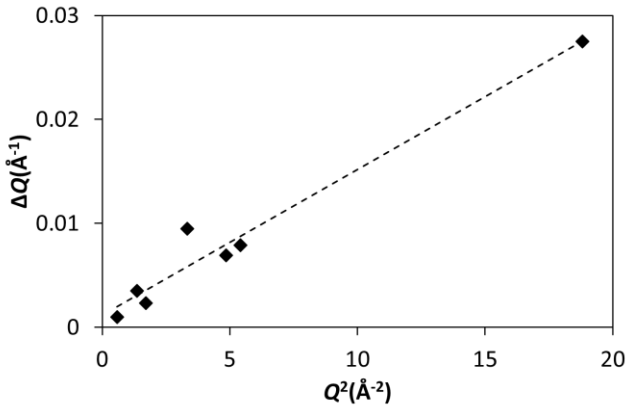

Figure 5: Peak width and position of the Bragg peaks for fluoro-apatite – mullite glass measured at 950°C. The dashed line is to guide the eye.

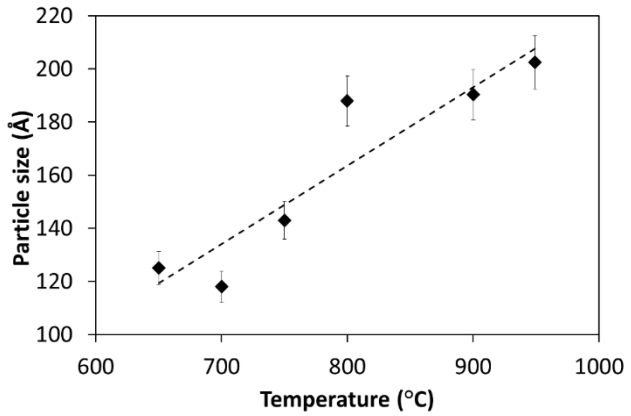

Figure 6: Crystallite size, estimated from the fitting of the Bragg peak occurring at 0.7 Å^{-1}, as a function of temperature. The dashed line is to guide the eye.

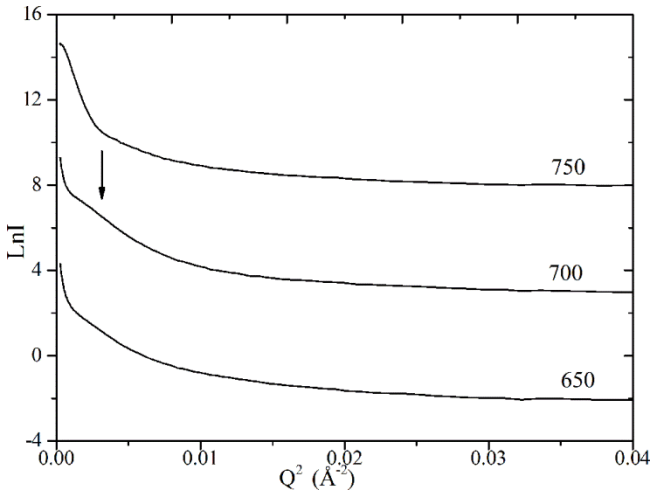

Figure 7. Guinier plot of the SANS data as a function of temperature. A small shoulder at ~0.003 Q^2 for the 700°C sample is indicated by the arrow.

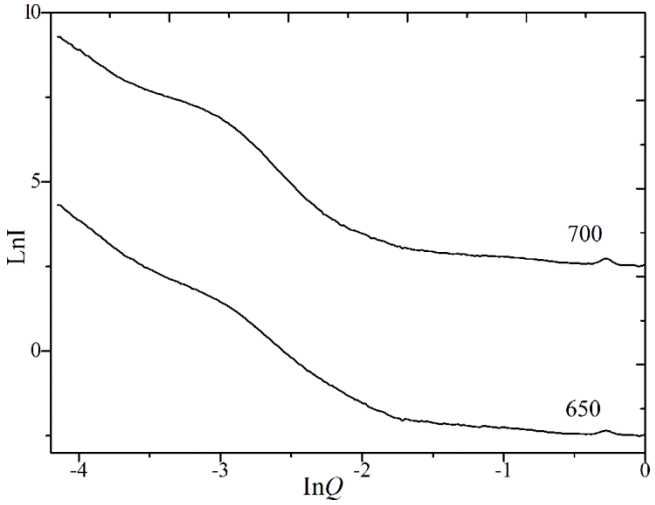

Figure 8. Porod plot of the SANS data at 650 and 700°C (offset by 5 for clarity).